Eur. Phys. J. D **55**, 279–285 (2009)
DOI: 10.1140/epjd/e2009-00101-2

THE EUROPEAN PHYSICAL JOURNAL D

Regular Article

Vision of nuclear physics with photo-nuclear reactions by laser-driven γ beams

D. Habs[1,2], T. Tajima[1], J. Schreiber[1], C.P.J. Barty[4], M. Fujiwara[3], and P.G. Thirolf[1,a]

[1] Faculty of Physics, Ludwig-Maximilians-University München, 85748 Garching, Germany
[2] Max-Planck Institute of Quantum Optics, 85748 Garching, Germany
[3] Research Center Nuclear Physics, Osaka University, Mihogaoka 10-1, Suita, Osaka 567-0047, Japan
[4] Lawrence Livermore National Laboratory, National Ignition Facility, 7000 East Avenue, Livermore CA 94550, USA

Received 22 November 2008 / Received in final form 13 February 2009
Published online 3 April 2009 –

Abstract. A laser-accelerated dense electron sheet with an energy $E = \tilde{\gamma}mc^2$ can be used as a relativistic mirror to coherently reflect a second laser with photon energy $\hbar\omega$, thus generating by the Doppler boost [A. Einstein, Annalen der Physik **17**, 891 (1905); D. Habs et al., Appl. Phys. B **93**, 349 (2008)] brilliant high-energy photon beams with $\hbar\omega' = 4\tilde{\gamma}^2\hbar\omega$ and short duration for many new nuclear physics experiments. While the shortest-lived atomic levels are in the atto-second range, nuclear levels can have lifetimes down to zeptoseconds. We discuss how the modulation of electron energies in phase-locked laser fields used for as-measurements [E. Goulielmakis et al., Science **317**, 769 (2007)] can be carried over to the new direct measurement of fs–zs nuclear lifetimes by modulating the energies of accompanying conversion electrons or emitted protons. In the field of nuclear spectroscopy we discuss the new perspective as a function of increasing photon energy. In nuclear systems a much higher sensitivity is predicted to the time variation of fundamental constants compared to atomic systems [V. Flambaum, `arXiv:nucl-th/0801.1994v1` (2008)]. For energies up to 50 keV Mössbauer-like recoilless absorption allows to produce nuclear bosonic ensembles with many delocalized coherent polaritons [G.V. Smirnov et al., Phys. Rev. A **71**, 023804 (2005)] for the first time. Using the $(\boldsymbol{\gamma}, \boldsymbol{n})$ reaction to produce cold, polarized neutrons with a focusing ellipsoidal device [P. Böni, Nucl. Instrum. Meth. A **586**, 1 (2008); Ch. Schanzer et al., Nucl. Instrum. Meth. **529**, 63 (2004)], brilliant cold polarized micro-neutron beams become available. The compact and relatively cheap laser-generated γ beams may serve for extended studies at university-based facilities.

PACS. 42.55.Vc X- and gamma-ray lasers – 29.27.-a Beams in particle accelerators – 41.75.Jv Laser-driven acceleration – 41.75.Ht Relativistic electron and positron beams

1 Introduction

In the case of photo-nuclear reactions nuclear transitions have been probed with keV–MeV photons arising from undulators at large storage rings, incoherent Compton backscattering of lasers from fast electron beams, or tagged photons from electron scattering. Here we point out the impact of coherently backscattered lasers from dense relativistic electron sheets, where we expect to harvess more intense and more brilliant keV–MeV photon beams. These brilliant photon beams will open up many new facets in nuclear physics.

Probing nuclei with intense and brilliant photon beams leads to many requirements on these beams, which are different from the cases of probing atoms.

The small size of nuclei with a few femtometer radius compared to Å of atoms results in very small dipole matrix elements and thus in much smaller interaction cross sections, integrated over the resonance width. The peak cross section $\sigma_{max} = \lambda^2/(2\pi)^2$ depends only on the γ wavelength λ and decreases with the square of the photon energy. Magnetic matrix elements are also small because of the small magnetic moments of nuclei. The ratio of the nuclear and atomic magnetic moments are approximately of order of the electron-to-proton mass ratio. Thus the decay lifetimes of nuclear levels are in general many orders of magnitude longer than the lifetimes of atomic levels for the same transition energy. A typical atomic transition of 1 eV with the full oscillator strength has a lifetime of ∼1 ns, while a nuclear E1 transition with 10 keV has a typical lifetime of picoseconds. Taking into account the $E_\gamma^{-(3-4)}$ scaling of the lifetime, atomic transitions for a 10 keV transition energy are typically $10^{\sim 10}$ faster than nuclear transitions. While typical atomic transitions are limited to ∼100 keV, nuclear transitions reach up to several MeV and thus can reach similar lifetimes in γ decay. Thus for nuclear spectroscopy the smallest possible

[a] e-mail: `Peter.Thirolf@physik.uni-muenchen.de`

bandwidth and a rather stable absolute energy of the γ beams is required.

While low-energy nuclear transitions are typically in the ns–fs range, lifetimes become much shorter when nuclear levels are particle unstable. Here lifetimes in the as–zs range are common. We wish to explore how the very successful streak camera technique for electrons from atomic systems [1,2] can be carried over to the streaking of protons in the proton decay of nuclei. Here two coherent photon fields with well-controlled relative phase are required. We have to discuss the situation, where two laser fields are reflected from a common relativistic mirror shifting the photons up in energy, while by the same factor shortening the pulse length of the reflected γ beams. While atomic transitions are limited to the attosecond (as) range – the lifetime of the K_α transition of uranium is 7 as and the atomic time unit $\tau = \hbar^3/me^4 = 24$ as – in nuclear physics lifetimes down to the zeptoseconds range (10^{-21} s) have been measured by looking at the Fourier-transformed energy width of transitions or measuring flight times. However, measuring decay times directly leads to a very different understanding of the processes compared to looking at the energy width. On the other hand, nuclear transitions have been measured electronically down to about 0.1 ps and extending the range for nuclear levels down to the zs-range by streaking techniques will result in a wealth of new nuclear spectroscopic information. The new techniques will also lead to many applications, because the suggested X-ray and γ-ray sources are rather compact devices, which will be cheap enough to be used in a small laboratory.

In this contribution we will describe the new method to produce brilliant X-rays and γ rays by reflecting laser beams from dense relativistic electron sheets. Then we will address the timing measurements by streaking. We will discuss the energy dependent spectroscopy of nuclei going from small to high γ energies. Finally we will address the possibility to produce cold micro-neutron beams.

2 The production of brilliant laser-driven γ beams

We pursue the new concept to drive a dense electron sheet out of an ultra-thin diamond-like carbon (DLC) foil [3], which we recently observed at the Los Alamos Trident laser facility [4]. The electron sheet is then accelerated within a half-cycle of the driver laser wavelength to its final energy $E = \tilde{\gamma}mc^2$ [5][1]. A second laser – the production laser – with photon energy $\hbar\omega$ is injected from the opposite direction of the electron direction. By performing a Lorentz transformation from the laboratory system to the rest frame of the electron sheet and then transforming for the reflected photon pulse back to the laboratory system, a Doppler boost with the final energy $\hbar\omega' = 4\tilde{\gamma}^2\hbar\omega$ is obtained [6]. It is important that the pulse front of the driver laser close to the focus can be tilted [7–9] as well as the target with respect to the driver laser propagation direction, so that is is possible to have the final momentum of the accelerated electrons orthogonal to the electron sheet surface and to have photons of the production laser injected opposite to the electron momentum direction. Then these photons are reflected opposite to the electron direction with maximum Doppler shift $4\tilde{\gamma}^2$.

The high density of the foil allows for efficient coherent reflection. The Coulomb expansion of the foil in the laboratory system is reduced by a factor of $\tilde{\gamma}^{-2}$, because longitudinally the Coulomb force of a charge is reduced by $\tilde{\gamma}^{-2}$ leading to a pancake-like field distribution [10]. Also the transverse expansion is reduced by a $\tilde{\gamma}^{-2}$, because the electron current leads to a $\boldsymbol{B}$ field encircling the beam, which via the $\boldsymbol{v} \times \boldsymbol{B}$ force transversely counteracts the electrical force, resulting that the total transverse expansion force is reduced by $\tilde{\gamma}^{-2}$. On the other hand the wave length λ of the counterpropagating laser is reduced in the inner rest frame by a factor of $\tilde{\gamma}$ and the distance d between electrons is increased by a factor of $\tilde{\gamma}$. Thus the ratio d/λ, which controls the number of coherently reflecting electrons is reduced by $\tilde{\gamma}^{-2}$. If we decrease the distance d of electrons by $\tilde{\gamma}^2$, the expanding forces in the laboratory and the number of coherently interacting electrons stay the same. This increase in density we can achieve by trapping the electrons of the sheet between the frontside and the backward laser. In this way an efficient relativistic reflection of the electron sheet is maintained for high $\tilde{\gamma}$ values. Moreover, the use of two lasers also prevents the longitudinal Coulomb expansion and smoothes the surfaces of the sheet.

The front laser can be viewed as an optical undulator. The backward acceleration laser acts like a "snowplough" and a density spike is building up, which preferentially reflects the front laser and thus a standing wave develops, which can lead to a micro-bunching of the electron sheet similar to FEL's. Even if this micro-bunching is incomplete due to the higher electron density, already a fractional micro-bunching is very helpful for the reflectivity. Comparing a classical FEL with an undulator period of 10 mm to our optical undulator with a period of 1 μm, we require about 10^2 times smaller electron energies for the same γ energy, because the optical undulator has a 10^4 times smaller wavelength. Furthermore the wavelength in the inner rest frame of the electron sheet is smaller and a micro-bunching has to be achieved over smaller distances. The much smaller electron sheet diameter is advantageous to weaken the requirements on the electron beam parameters. This concept has been described in more detail in reference [11].

Similar to other concepts of reflecting relativistic mirrors [12,13], the mirror can be shaped by the lasers in order to obtain a focussing effect, making the approach very efficient. In this way the high intensities can be achieved that are required for streaking protons. The concept will work best at lower photon energies like 10 keV, where the reflectivity is high from the beginning, without relying on laser trapping and micro-bunching.

[1] We introduce $\tilde{\gamma}$ as scaling factor for the energy to differentiate it from the γ used e.g. for γ beams.

Since we often need γ beams in nuclear physics with small bandwidth, the reflected laser with N cycles will have a bandwidth $\propto 1/\sqrt{N}$. If the reflected photons lead to a deceleration of the electron sheet and a chirp of the reflected γ beam, a compensating chirp of the optical laser would be required. The driving laser, which leads to the breakout of the electrons from the foil and the acceleration within a half-cycle, should be a few-cycle laser pulse. For this laser the large bandwidth and a good compression with a high contrast is difficult to achieve simultaneously.

We will learn more on the properties of the relativistic electron sheet by simultaneously reflecting two laser beams with different photon energies. In this way their reflectivities and their phase relations can be studied.

In the end a lot of relativistic engineering [14] and fine tuning of the lasers and foil-target technology are required to achieve the optimum properties of the γ beams.

At the end of this section we want to compare the expected brilliant γ-rays from laser driven relativistic mirrors for nuclear physics with γ beams produced with classical electron beams. We take as example the high intensity gamma-ray source (HIγS) at Duke University (USA), where intense XUV-FEL photons are incoherently backscattered from electron bunches of a storage ring with electron energies of 300–1200 MeV [15]. Furthermore we consider the low-energy photon tagger NEPTUN of the electron linac S-DALINAC in Darmstadt (Germany), where γ-photons from a radiator are tagged by measuring the coincident electron energy loss in a focal plane detector [16].

The numbers of Table 1 show that the expected γ-beam properties produced with the relativistic electron mirror are many orders of magnitude superior in γ flux and γ-beam quality compared to the classically produced γ beams. Furthermore, the laser-driven facility is much more compact and cheaper, opening hopefully a new era of university-based nuclear physics.

Table 1. Comparison of γ beams produced from classical electron beams and laser-driven relativistic electron mirrors for nuclear physics experiments.

	Rel. γ-mirror	HIγS	Neptun
E_{electron}	0.01–2 GeV	0.3–1.2 GeV	30 MeV
γ range	1 keV–50 MeV	2–50 MeV	6–20 MeV
prod. laser	optical	XUV FEL	–
γ-range	0.01–50 MeV	2–50 MeV	6–20 MeV
γ-rate	10^{13}/s	10^{7}/s	10^{5}/s
E_γ spread	10%	1%	0.3%
γ-beam	coherent	incoherent	incoherent
γ-duration	10^{-21}–10^{-15} s	10^{-12} s	10^{-9} s
γ-beamsize	$\sim$1 μm	$\sim$1 mm	$\sim$1 mm
polaris.	switchable	switchable	–
γ-backg.	–	–	untagged γ's

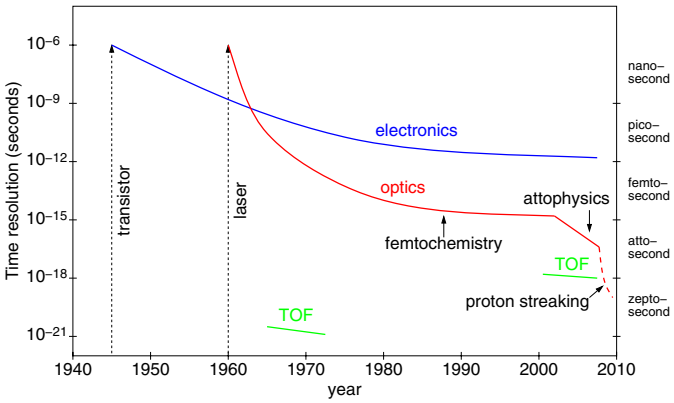

Fig. 1. (Color online) Time resolution as a function of years, achieved with electronic, optical, and time-of-flight techniques.

3 Nuclear lifetime measurements by streaking

Many techniques have been developed to measure nuclear lifetimes:

(1) with electronic techniques lifetimes down to ps can be measured [17];
(2) lifetimes in the 10^{-16} s range could be measured [18] by comparing the lifetime of proton emission and K X-ray emission, thus using the X-rays as an atomic clock, while observing which fraction of the proton decay left the nucleus before or after the X-ray emission through a coincidence measurement of the X-ray energy;
(3) in a similar way nuclear clocks have been used in the 10^{-18} s time range or as-range [19];
(4) lifetimes in the range of 10^{-18} s were also studied by investigating the blocking of channeling of fission fragments in aligned crystals – a kind of time-of-flight (TOF) measurement in the Å-range of flight lengths [20,21];
(5) very short lifetimes in the 10^{-21} s range or zs-range could be measured by proximity scattering, another time-of-flight (TOF) measurement in the fm-range of flight lengths [22–24].

Figure 1 shows the achieved time resolutions as a function of the corresponding year for different techniques. While electronic techniques are limited to about a picosecond, now optical methods using streaking techniques reach into the attosecond range. Also with time-of-flight (TOF) techniques with traveling distances in the Å or fm range, very short lifetimes can be probed.

Figure 2 shows some nuclear lifetimes as a function of the excitation energy above the ground state. In comparison also typical atomic lifetimes as a function of level energy are shown. Though detailed theories on nuclear lifetimes have been developed, we want to give some order of magnitude estimates. Single particle half-lives for γ-decay including contributions from internal conversion for E1 transitions are given by [25]:

$$T^{\gamma}_{1/2}(s) = 6.76 \times 10^{-6}/(E^3_\gamma \times A^{2/3}) \quad (1)$$

and for M1 transitions by:

$$T^{\gamma}_{1/2}(s) = 2.20 \times 10^{-5}/E^3_\gamma \quad (2)$$

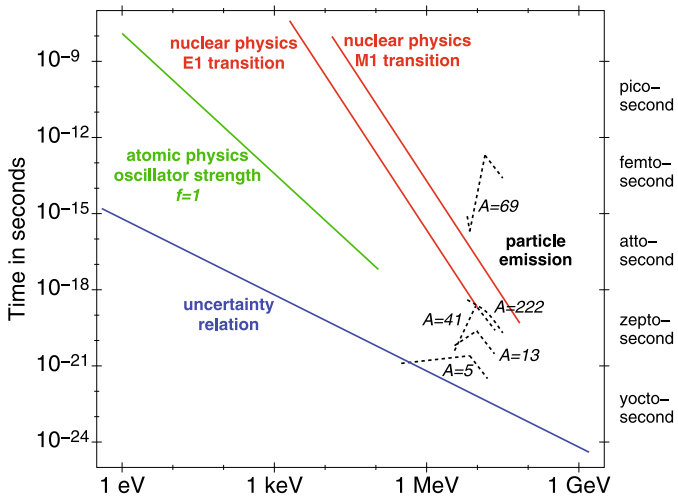

Fig. 2. (Color online) Correlation between time and energy. The curve in green corresponds to atomic levels with oscillator strength $f = 1$, the red curves represent single particle estimates for nuclear E1 and M1 γ transitions, while the blue line denotes the limit given by the uncertainty relation. The dashed black lines indicate lifetimes of nuclear levels after particle emission for different mass numbers A.

where the transition energies are given in keV. These E1 and M1 half-lives are shown in Figure 2 for $A = 120$. For the much faster particle emission the lifetime T_p can be calculated within the optical model, using a transmission coefficient T and the level density ρ for lower isolated resonances [26]:

$$T_p = 2\pi\rho/T. \tag{3}$$

The density $\rho(E)$ may be estimated from a simple formula:

$$\rho(E) = \rho(0)e^{\sqrt{2(aE)}} \tag{4}$$

where $\rho(0)$ and a are given as a function of mass number A and typical values for $A = 120$ are $\rho(0) = 0.02$ MeV^{-1} and $a = 8$ MeV^{-1} [27]. The calculation of transmission coefficients is explained in reference [26]. Particle emission lifetimes between 10^{-16}–10^{-21} s have been measured. After a rise of the lifetime with excitation energy a decrease of the lifetime with excitation energy sets in because the resonances start to overlap and their widths spread. Thus damping widths become important. One can introduce a temperature $kT = \sqrt{E_{ex}/a}$ for a nucleus with excitation energy E_{ex}. With the emission of particles a cooling effect, or a decrease of the excitation energy E_{ex} and the temperature T occurs. Until now only time integrated particle spectra have been measured and it was not possible to measure the particle spectra as a function of emission time. Typical particle emission times in the range of 10^{-20} s are obtained from statistical model calculations for higher excitation energies [28]. If it were possible to follow the emission spectra as a function of time, a much better understanding of dissipation and damping processes could be obtained.

Furthermore, laser pulses are boosted by a factor of $4\tilde{\gamma}^2$ in energy and are reduced in duration by a factor $1/(4\tilde{\gamma}^2)$. For a single cycle pulse the energy versus time relation would be described by the uncertainty principle. This demonstrates that excitations with γ pulses much shorter than the expected lifetimes are possible.

Though many methods have been developed in different time ranges for different decays, transfering the streaking techniques of atomic physics to nuclear physics will give access to a new disentanglement of the processes where all complex energy spectra could be followed as a function of time.

3.1 Streaking of conversion electrons

Nuclear levels below the particle emission threshold (∼6–8 MeV) not only decay by γ emission but also are accompanied by prompt conversion electrons with a fraction given by the conversion coefficient. The dominant peaks in the conversion electron spectrum are the K-conversion lines.

Now we excite a level of a stable nucleus with a γ beam of suitable energy. In parallel we superimpose a laser field to the nucleus with a tunable delay between the photonuclear excitation and the streaking field of the conversion electron. The energy modulation of the conversion electron should be in the range of 5 keV, requiring laser intensities of 10^{14} W/cm^2. With a magnetic transport and filter system ('Mini-Orange' spectrometer) for conversion electrons [29] we can choose the transmission curve to select a narrow range of the conversion electron spectrum with high efficiency, while fully suppressing all electrons being directly accelerated from atomic shells. By varying the delay of the streaking field, lifetimes in the range of 1–100 fs can be measured. For the release of the conversion electrons we need γ beams of 10 keV–5 MeV. Metallized tapes with stable target nuclei would be ideal targets. The measurements would allow to determine the spins and parities of the excited levels. From the transition matrix elements many properties of their wave functions could be deduced.

3.2 Streaking protons from the (γ, p) reaction to measure lifetimes of nuclear levels in the 7–10 MeV excitation energy range

For nuclear levels at excitation energies of 7–10 MeV we expect lifetimes in the 100 as–zs range, where proton-rich nuclei emit rather low-energy protons.

Thus the streaking field should lead to modulations of the proton energy of about 10 keV. To measure these shorter lifetimes, a laser field with an oscillation frequency of a few attoseconds or 10 keV photons would be suitable with a field strength in the range of 10^{22} W/cm^2 and a normalized vector potential a of 10^{-1}. Such a field strength corresponds (diffraction-limited) to 10^5 photons, while we expect to produce 10^{13} photons. Thus the 10 keV beam may be focused to a volume of (500 Å)^3, thus containing many nuclei. With a second γ beam from the same relativistic mirror the excitation of the nuclear levels in the 7–10 MeV range is performed.

We envisage a stepwise development of this technique, studying first the (γ, p) reaction and the streaking of low-energy protons.

4 Nuclear spectroscopy with rather monoenergetic γ beams

4.1 The 7.6 eV transition of ^{229}Th

The lowest known first excited nuclear level occurs in ^{229}Th. Recently its excitation energy was measured with a cooled X-ray microcalorimeter and an excitation energy of 7.6 ± 0.5 eV was obtained [30], corresponding to a wavelength of 163 ± 11 nm. For this transition we exemplarily want to explain the differences between atomic and nuclear photon transitions and their perspectives. From the nuclear matrix elements of similar levels in neighbouring nuclei a lifetime of ∼3–5 h can be predicted for ^{229m}Th, resulting in an extremely small energy width of $\Delta E/E \sim 10^{-20}$. Our aim is to measure this transition energy much more accurately. In a first step we want to determine the transition energy to about 10^{-4} with sharply-absorbing filters [31], where we populate the 7.6 eV isomer in the α decay of ^{233}U. Since the measured transition energy recently was revised from 3.5 eV to 7.6(5) eV [30], all previous studies searched at the wrong transition energy and thus failed. In a second step we want to excite the transition with a very monochromatic dedicated laser. Here it was proposed to detect the nuclear excitation by shelving of an atomic cyclic transition [32]. Therefore we are setting up a sympathetic cooling scheme of $^{229}Th^{3+}$ by laser-cooled $^{24}Mg^{+1}$ ions. By using this 3^+ charge state we obtain a very simple electronic level scheme (Rn core and a single valence electron) and we avoid the so-called electronic bridge processes, where the isomeric nuclear energy may be transferred to an outer electron [33].

In theories that unify the standard model with gravity one expects a time variation of the fundamental "constants" (like the fine structure constant α or the strong interaction parameter Λ) for the expanding universe. The main importance to study this ultra-stable nuclear clock transition is that an up to 10^{10}-fold increase in sensitivity is predicted for the 7.6 eV transition in ^{229}Th when studying a potential time-dependence of fundamental constants, compared to atomic transition measurements [34].

This shows that nuclear transitions due to the small nuclear dimensions are very sensitive to such changes and nuclei are much better shielded against external perturbations, due to the much smaller matrix elements and the shielding electronic cloud. Thus nuclear spectroscopy of very different fundamental properties will be enabled, allowing to explore especially the hadronic interaction with very high precision.

4.2 Coherent ensembles of Mössbauer nuclei

For nuclear transitions up to 100 keV the recoilless Mössbauer absorption has been observed. For bound nuclei the photon recoil may be taken up by the crystal without lattice excitation. A prototype nucleus is ^{57}Fe with its 14.4 keV Mössbauer M1 transition, which has a mean lifetime of 141 ns, a line width of 4.7 neV, a relative line width of $\Delta E/E = 3 \times 10^{-13}$ and a K-conversion coefficient $\alpha_K = 10$. At synchrotron facilities the non-resonant radiation could be suppressed sufficiently by nuclear Bragg reflection. Here the delocalized excitation of a nuclear ensemble – called nuclear polariton [35] – was studied in detail. Its delayed propagation through a crystal, showing quantum beats due to the interference of different transitions between hyperfine components was observed. This coherent γ-ray optics shows many new phenomena [36]. Although the brilliance of synchrotron γ beams much increased over the years, at most one nuclear polariton could be produced in a target. With our new increased peak brilliances of laser-driven X-ray beams it appears possible to produce $N_p = 10^3$ coherent polaritons in an ensemble of nuclei. Thus a new world of coherent effects of many polaritons becomes accessible. The decay rate or γ width is increased by N_p and soon exceeds the width due to conversion. Then an avalanche-like growth of the linewidth occurs and more and more photons of the much broader driving X-ray beam may join the polariton condensate. Studying the collective properties of these bosonic condensates opens up a perspective of coherent nuclear physics.

4.3 The photonuclear resonance reaction

For high photon energies the Mössbauer effect is no longer applicable, but still photonuclear resonances have extremely small line widths. The lines are broadened by the thermal Doppler shift with:

$$\Delta E/E \sim 10^{-6}\sqrt{(kT/25\ \mathrm{meV})(240/A)} \qquad (5)$$

here new techniques are used to detect the narrow resonances with high sensitivity: a 'notch' detector measures the absence of resonance photons [37–39]. A γ beam with narrow energy width, including the resonance energy of interest, is passed through a sample. The isotope of interest burns an extremely narrow hole into the γ beam by scattering out the resonance photons. This depletion of resonance photons – called 'notch' – is detected by placing an additional probe of the expected isotope into the beam with the notch and measuring the resonance scattering together with the off-resonance photons. In this way a depletion of the resonance line due to the sample is detected, using the very high resolution of nuclear resonance scattering. Here the new brilliant, polarized, high-energy γ beams are very useful, because they penetrate thick samples and allow the detection of very small amounts of isotopes. This method is proposed to detect e.g. ^{235}U , ^{239}Pu [38] or relevant isotopes of nuclear waste, but also for the detection of clandestine nuclear materials. The nuclear resonance fluorescence scattered sidewards can be measured with a high-purity Ge detector to study radioactive waste drums non-intrusively [38]. The sensitivity of detecting the U and

Pu waste is improved using M1 transitions due to the directional orientation of the decay photons after the nuclear fluorescence with polarized γ beams.

4.4 Parity violating nuclear transitions

The γ beams reflected from relativistic dense electron sheets allow for an easy switching of the polarization by switching the polarization of the primary reflected laser beam. This switching between rather pure polarizations can be the basis for further interesting nuclear fluorescence studies.

A series of experiments has been performed, studying the parity non-conservation in nuclear resonance fluorescence from nuclei having close-lying parity-doublet states. According to first order perturbation theory calculations, the measured asymmetry is strongly enhanced, because the parity violating matrix element is divided by the small energy difference of the two levels of opposite parity. Here many nuclei with a possible E1/M1 mixing have been investigated (^{18}F (1080 keV); ^{19}F (109.9 keV); ^{21}Ne (2789 keV); ^{175}Lu (396 keV)), but experimental accuracies were insufficient. Thus for ^{21}Ne the level distance between the $1/2^+$ and $1/2^-$ states is only 5.7 keV, leading to a large enhancement effect. Here the Seattle group reported an asymmetry of $(0.8 \pm 1.4) \times 10^{-3}$ [40]. With the new brilliant γ beams the situation may improve. In this way elementary parity-violating meson-nucleon coupling constants can be determined [41–44].

5 Are pump-probe experiments possible in nuclear physics?

In nuclear physics we face the severe problem that large nuclear cross sections are only typically 100 mb ($=10^{-25}$ cm^2), while in atomic physics large cross sections are Å^2 $= 10^{-16}$ cm^2, showing that it is difficult to excite the same nucleus in a pump-probe experiment twice. A way out is to find methods of locally exciting the nucleus in the first step with a very intense current. One proposal is to use two counterpropagating laser beams [45], where the $(\boldsymbol{v} \times \boldsymbol{B})$ terms cancel and thus one can use the high local K-electron density at the nucleus to drive efficiently Coulomb excitation with these electrons of many MeV. It is clear that the much higher required intensities ask for a much smaller interaction volume and thus for shorter wavelengths of the γ beams. In a second step the broadband excited nuclei can be probed by an additional γ beam looking e.g. for a characteristic fission signature from the first, second or third minimum of the potential energy surface of heavy nuclei after giant resonance excitation [46].

6 A thermal micro-neutron source via the (γ, n)-reaction

In a similar way as we have discussed the streaking measurements for the (γ, p) reaction, we want to explore the

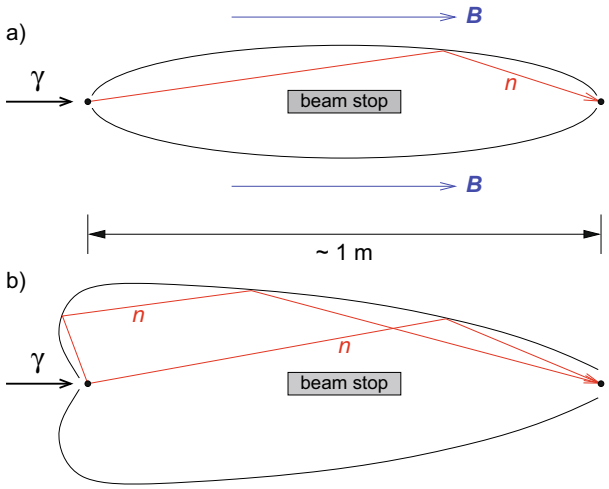

Fig. 3. (Color online) (a) Focusing for thermal neutrons; (b) when taking the neutron-energy neutron-angle relation into account, a more efficient neutron focusing system can be designed. For neutron spin echo techniques B-fields can be superimposed to the focusing device.

(γ, n) reaction for heavy nuclei to produce thermal neutrons. In both reactions the low energy tail of the giant resonance will enhance the γ excitation cross section. From the time reversed (n, γ) reaction we know for thermal neutrons the Γ_n- and Γ_γ-widths and the level densities at the neutron binding energy (B_n). However, while the (n, γ) reaction populates in parallel many γ cascades, feeding also many excited levels, here we are only interested in excitations from the ground state. A first step in neutron production is to measure the yield, the energy distribution and the angular distribution of the neutrons by using the time of flight method for the neutrons. Due to the photon recoil the capturing heavy nucleus will acquire an energy of about 70 eV. Thus on the average a momentum of 25 keV/c is superimposed in γ direction onto the neutrons emitted in the rest frame of the heavy nucleus. Since we are interested in thermal neutrons with a typical energy of 40 meV, we have to populate resonances just 300 eV above the neutron binding energy and select neutrons emitted opposite to the γ direction. At these excitation energies of 6 MeV of heavy nuclei a typical level spacing amounts to 5 eV, a maximum $\Gamma_{\gamma 0}$-width to the ground state of ~20 meV and a typical neutron width Γ_n of ~1 meV. Exploring the neutron resonances of stable heavy isotopes at about 300 eV above the neutron binding energy will be an important task. Our aim is to directly produce thermal neutrons and to avoid the moderation process of present large-scale neutron sources, which leads to large average diameters (~1 m) of thermal sources. By placing the production source with a diameter of Å size into the focal spot of an ellipsoidal imaging system [47,48], only the thermal neutrons within a cone of 10 degree are imaged into the opposite focal point with one neutron reflection, while the direct vision between the two focal spots is blocked. Since we have a strong correlation between neutron energy and angle, the efficiency of the transport system is estimated to be better than 10 degree acceptance angle. Perhaps a

kind of adaptive neutron optics with actuators could be used for the neutron optics device to improve the neutron spot size.

With polarized γ rays polarized neutrons are produced, where spin echo techniques can be superimposed to the imaging system. Due to the very accurate γ-start signal the neutron energies after elastic or inelastic scattering can be measured via time-of-flight, while elastic and inelastic reactions can be separated by the spin echo technique. Thus in the second focus a clean, tagged thermal micro-neutron is produced, without requiring a large reactor or spallation source. However, we have to demonstrate that we reach a competitive neutron flux of 10^8/s. This certainly requires the production of γ beams with about 6 MeV with a very small line width.

7 Conclusions

We have introduced several examples of photo-nuclear physics problems that may be tackled with the emergent bright γ beams driven by intense laser pulses. While we try to reach shortest pulses for atomic physics and structure diagnostics of large molecules with photon energies below 100 keV, we are interested in nuclear physics for γ energies below 6 MeV with smallest bandwidth. For energies above 6 MeV, due to the fast particle decay of nuclei, we are again interested in shortest pulses.

With respect to the energy of X-rays and γ beams for structural analysis probably the energy range of 10–50 keV is the best. For 50 keV we find in biological tissue the least dose deposition [49], being optimal for medical diagnostics. We are performing at the ESRF phase contrast imaging of full breast and cartilage samples. Here the grid based imaging [50] appears best suited for the new laser driven X-ray sources. For nuclear physics a broad energy range from 10 keV to a few MeV is of interest.

Nuclear physics has many applications from radioactive waste management to homeland security, which partly were addressed in Section 4.3. Here the compact, comparably cheap laser-driven γ-beam facilities will have a bright future.

We acknowledge many useful discussions with P. Böni and U. van Bürck. Supported by Deutsche Forschungsgemeinschaft through the DFG-Cluster of Excellence Munich-centre for advanced photonics (MAP) and Transregio TR18. The authors acknowledge the support by the European Commission under contract ELI pp 212105 in the framework of the program FP7 Infrastructures-2007-1.

References

1. E. Goulielmakis et al., Science **317**, 769 (2007)
2. J. Itatani et al., Phys. Rev. Lett. **88**, 173903 (2002)
3. O. Klimo et al., Phys. Rev. ST Accel. Beams **11**, 031301 (2008)
4. D. Kiefer et al., Eur. Phys. J. D **55**, 427 (2009)
5. V.V. Kulagin et al., Phys. Rev. Lett. **99**, 123801 (2007)
6. A. Einstein, Annalen der Physik **17**, 891 (1905)
7. A.K. Sharma et al., Opt. Express **14**, 13131 (2006)
8. S. Akturk et al., Opt. Express **12**, 4399 (2004)
9. Z. Sacks et al., Opt. Lett. **26**, 462 (2001)
10. J.H. Jackson, *Classical Electrodynamics* (John Wiley, New York, 1972), p. 556
11. D. Habs et al., Appl. Phys. B **93**, 349 (2008)
12. A.S. Pirozhkov et al., Phys. Plasmas **14**, 123106 (2007)
13. A.V. Panchenko, T.Z. Esirkepov, A.S. Pirozhkov, M. Kando, F.F. Kamenets, S.V. Bulanov, submitted to Phys. Plasmas
14. T. Tajima, Eur. Phys. J. D **55**, 519 (2009)
15. H.R. Weller, M. Ahmed, Mod. Phys. Lett. A **18**, 1569 (2003)
16. K. Lindenberg, thesis, *Development and Construction of the Low-Energy Photon Tagger NEPTUN*, TU Darmstadt, 2007
17. H. Mach et al., Nucl. Instrum. Meth. A **280**, 49 (1989)
18. J.C. Hardy et al., Phys. Rev. Lett. **37**, 133 (1976)
19. D. Hilscher et al., Ann. Phys. (Paris) **17**, 471 (1992)
20. J.U. Anderson et al., Phys. Rev. Lett. **99**, 162502 (2007)
21. S.A. Karamian et al., Eur. Phys. J. A **17**, 49 (2003)
22. J. Lang et al., Phys. Lett. **15**, 248 (1965)
23. S. Kato et al., Nucl. Phys. A **195**, 534 (1972)
24. L. Lassen et al., Phys. Lett. B **24**, 338 (1967)
25. R.B. Firestone et al., *Table of Isotopes*, Vol. 2 (John Willey & Sons, New York, 1996)
26. J.M. Blatt, V.F. Weisskopf, *Theortical Nuclear Physics* (John Wiley, New York, 1952), p. 389
27. E. Segre, *Nuclei and Particles* (W.A. Benjamin, Inc., New York, 1965)
28. P. Paul, M. Thoennessen, Annu. Rev. Nucl. Part. Sci. **44**, 65 (1994)
29. J. van Klinken, K. Wisshak, Nucl. Instrum. Meth. **98**, 1 (1972); J. van Klinken, S.J. Feenstra, K. Wisshak, H. Faust, Nucl. Instrum. Meth. **130**, 427 (1975); J. van Klinken, S.J. Fenstra, G. Dumond, Nucl. Instrum. Meth. **151**, 433 (1978)
30. B.R. Beck et al., Phys. Rev. Lett. **98**, 142501 (2007)
31. P.G. Thirolf et al., *Optical access to the lowest nuclear transition in* ^{229m}*Th*, MLL anual report 2007, p. 8
32. E. Peik et al., Europhys. Lett. **61**, 181 (2003)
33. F.F. Karpeshin et al., Hyperfine Interact. **162**, 125 (2005)
34. V. Flambaum, `arXiv:nucl-th/0801.1994v1` (2008)
35. G.V. Smirnov et al., Phys. Rev. A **71**, 023804 (2005)
36. J.P. Hannon et al., Hyperfine Interact. **123/124**, 127 (1999)
37. W. Bertozzi et al., Nucl. Instrum. Meth. B **241**, 820 (2005)
38. W. Bertozzi et al., Phys. Rev. C **78**, 041601(R) (2008)
39. J. Pruet et al., J. Appl. Phys. **99**, 123102 (2006)
40. E.D. Earle et al., Nucl. Phys. A **339**, 221c (1983)
41. A.I. Titov, M. Fujiwara, K. Kawase, J. Phys. G **32**, 1097 (2006)
42. W.C. Haxton et al., Phys. Rev. Lett. **86**, 5247 (2001)
43. W.C. Haxton et al., Phys. Rev. C **65**, 045502 (2003)
44. E.G. Adelberger et al., Annu. Rev. Nucl. Part. Sci. **35**, 501 (1985)
45. N. Milosevic et al., Phys. Rev. Lett. **92**, 013002 (2004)
46. P.G. Thirolf, D. Habs, Prog. Part. Nucl. Phys. **49**, 325 (2002)
47. P. Böni, Nucl. Instrum. Meth. A **586**, 1 (2008)
48. Ch. Schanzer et al., Nucl. Instrum. Meth. **529**, 63 (2004)
49. R.A. Lewis, Phys. Med. Biol. **49**, 3573 (2004)
50. F. Pfeiffer et al., Nature Phys. **2**, 258 (2006)
51. S.V. Bulanov et al., Phys. Rev. Lett. **91**, 085001 (2003)